Published in final edited form as:
Anat Rec (Hoboken). 2009 July ; 292(7): 1045–1061. doi:10.1002/ar.20921.

Peroxisome Proliferator-Activated Receptor-γ Agonist Treatment Increases Septation and Angiogenesis and Decreases Airway Hyperresponsiveness in a Model of Experimental Neonatal Chronic Lung Disease

K. Takeda[6], **M. Okamoto**[6], **S. De Langhe**[6], **E. Dill**[6], **M. Armstrong**[5], **N. Reisdorf**[5], **D. Irwin**[1], **M. Koster**[5], **J. Wilder**[7], **K.R. Stenmark**[1,4], **J. West**[8], **D. Klemm**[1,2,4], **E.W. Gelfand**[5], **E. Nozik-Grayck**[1,4], and **S. M. Majka**[1,3,5,*]

[1] Cardiovascular Pulmonary Research Lab, University of Colorado Denver Health Science Center

[2] Division of Pulmonary Sciences & Critical Care Medicine, University of Colorado Denver Health Science Center

[3]Department of Medicine, Cardiology Division, University of Colorado Denver Health Science Center

[4] Division of Critical Care Medicine; Department of Pediatrics, University of Colorado Denver Health Science Center

[5] Gates Center for Regenerative Medicine and Stem Cell biology, University of Colorado Denver Health Science Center

[6] National Jewish Health, Department of Pediatrics, Division of Cell Biology

[7]Lovelace Respiratory Institute, Albuquerque NM

[8]Division of Allergy, Pulmonary, and Critical Care Medicine, Vanderbilt University, Nashville, Tennessee

Abstract

Chronic lung disease (CLD) affects premature newborns requiring supplemental oxygen and results in impaired lung development and subsequent airway hyperreactivity. We hypothesized that the maintenance of peroxisome proliferator-activated receptor gamma (PPARγ) signaling is important for normal lung morphogenesis and treatment with PPARγ agonists could protect against CLD and airway hyperreactivity (AHR) following chronic hyperoxic exposure. This was tested in an established hyperoxic murine model of experimental CLD. Newborn mice and mothers were exposed to room air (RA) or moderate hyperoxia (70% oxygen) for 10 days and fed a standard diet or chow impregnated with the PPARγ agonist rosiglitazone (ROSI) for the duration of study. Following hyperoxic exposure (HE) animals were returned to RA until postnatal day (P) 13 or P41. The accumulation of ROSI in neonatal and adult tissue was confirmed by mass spectrometry. Analyses of body weight and lung histology were performed on P13 and P41 to localize and quantitate PPARγ expression, determine alveolar and microvessel density, proliferation and alpha-smooth muscle actin (α-SMA) levels as a measure of myofibroblast differentiation. Microarray analyses were conducted on P13 to examine transcriptional changes in whole lung. Pulmonary function and airway responsiveness were analyzed at P55. ROSI treatment during HE preserved septation and vascular density. Key array results revealed ontogeny groups

[*]to whom correspondence should be directed: University of Colorado Health Science Center, SOM 3810, Mail stop B-133, 12700 E 19th Ave, Aurora, Colorado 80045; Susan.majka@ucdenver.edu, Ph: (303) 883 8786; Fax: (303) 724 3051.

differentially affected by hyperoxia including cell cycle, angiogenesis, matrix and muscle differentiation/contraction. These results were further confirmed by histological evaluation of myofibroblast and collagen accumulation. Late AHR to methacholine was present in mice following HE and attenuated with ROSI treatment. These findings suggest that rosiglitazone maintains downstream PPARγ effects and may be beneficial in the prevention of severe CLD with AHR.

Keywords

Chronic Lung Disease (CLD); Rosiglitazone; PPAR gamma; Lung simplification; airway hyperresonsiveness (AHR)

Introduction

In prematurely born infants the alveoli and pulmonary blood vessels are not fully developed leading to impaired gas exchange and risk for RDS. These infants are at risk for respiratory distress syndrome (RDS), a condition which results in inefficient oxygen and carbon dioxide exchange at the alveolar-capillary level (7 10 14 37 41). RDS is treated with oxygen and/or mechanical ventilation, which can be life-saving but may result in detrimental side effects that include hyperoxic lung injury, barotrauma and infection (7 10 14 41 45). Collectively, these conditions lead to impaired lung development and chronic lung disease (CLD) (7 45). Bronchopulmonary dysplasia (BPD) is the most common chronic lung disease of infancy (45). A common late sequelae of CLD is reactive airway disease (10 14 45).

Mechanisms that protect against oxidative damage, inflammation and atelectasis are essential to preserve normal lung development. Peroxisome proliferator-activated receptors (PPARs) have emerged as essential regulators in these processes (3 17 25-29 36 37). These nuclear receptors include the transcription factor PPAR-α, involved in the regulation of energy homeostasis, fatty acid catabolism, and gluconeogenesis and PPAR-β/δ, implicated in the regulation of fatty acid oxidation (3 4 30 44). Another isoform, PPAR-γ mediates the expression of genes important in cellular metabolism and differentiation (16 21 29 39 43). In the lungs, PPAR-γ is expressed in multiple cell types including monocytes, endothelial and smooth muscle cells where it regulates proliferation and vascular tone (1 2 5 16 18 21). Postnatal ablation of PPAR-γ in the rodent airway epithelium disrupts development resulting in enlarged airspaces and decreased tissue resistance (28 29). Studies have indicated that PPAR-γ is capable of maintaining the lipofibroblast versus myofibroblast phenotype, have anti-inflammatory activity and are potential antifibrotic agents (3 6 11 13 20 22 25-27 32 36 40). The appearance of myofibroblasts and their proliferation are key events in the development of CLD. PPARγ is activated by both natural (fatty acids, eicosanoids and prostaglandins (15d-PGJ_2) and synthetic thiazolidinediones (TZDs): troglitazone, ROSI, ciglitazone, and pioglitazone) compounds (15 16). In recent years, TZD drugs have been tested for their ability to block fibroblast differentiation and smooth muscle cell proliferation in various disease models (11 15 22 26 36). The role of PPARγ agonists in CLD and their effects on developing lungs has not been well defined.

We hypothesized that restoring PPARγ activity with the agonist ROSI could protect against experimental CLD and long-term airway hyperresponsiveness (AHR). We employed a novel strategy using a murine model of chronic moderate hyperoxia leading to morphometric and airway hyperreactivity characterisitic of CLD. Neonates received systemic delivery of ROSI through their mothers' diet, shown by detection of drug in milk. ROSI treatment upregulated multiple PPAR-γ target genes in the neonatal lungs. Drug treatment offset the adverse effects of hyperoxic exposure to the neonates by increasing alveolar and vascular density

and attenuating late AHR. We conclude that the maintenance of PPAR-γ activity through dietary supplementation during late stages of lung development is crucial to lung morphogenesis and may be evaluated as a therapeutic target to treat CLD.

Methods

Mouse Model of CLD

C57Bl/6 mice were purchased from The Jackson Laboratory (Bar Harbor, ME) and housed in the UCDHSC/Webb Waring central vivarium under pathogen free conditions. All procedures were performed according to the Animal Care and Use Committee guidelines at UCDHSC. Newborn mice (P0-P1 days of age) were exposed to room air (RA, RA+ROSI) or 70% oxygen (HE, HE+ROSI) for 10 days. Mice were exposed to constant flow oxygen in plexiglass chambers housing the cages while delivery of oxygen was continually monitored using a Pro-ox sensor (19). Following 10 days of RA or hyperoxic exposure, mothers and neonates were placed at room air (relative normoxia at Denver altitude). Animals were studied at postnatal day 13 and 41 (3 and 31 days following hyperoxic exposure). At this level of hyperoxia, dams body weight was not affected and no detriment to their health or pups was noted, therefore dams were not rotated between normoxia and hyperoxia. These findings were in contrast to exposure to higher oxygen, which is toxic and requires dam rotation.

The lungs of newborn mice form P0-P5 are in the late terminal saccular phase of development, similar to preterm human infants At the time of sacrifice, age, total body weights and heart weights were recorded. Mice were studied at postnatal day 13 and 41. At each age, there were four experimental groups: Room air (RA), RA+ Rosiglitazone (ROSI), Hyperoxic exposed (HE), and HE + ROSI. The numbers of animals studies per group were as follows: Postnatal (P) day 13: Room air (RA) n=12; RA+ROSI n=7, Hyperoxic exposed (HE) n=15; HE+ROSI=10. P41: RA n=15; RA+ROSI n= 6; HE n=15; HE+ROSI=12.

Rosiglitazone treatment of neonatal mice—To study the effects of PPARγ select mothers exposed to RA or HE were fed PPARγ ligand, Rosiglitazone (ROSI), impregnated chow (2.5-10 mg/kg/day) or regular chow from P0 until P41. ROSI impregnated chow at this dose has been shown to have a systemic effect on fat differentiation and smooth muscle cell proliferation (12) and indirect drug delivery via dams' milk is commonly used for drugs secreted into breast milk such as doxycycline (48). ROSI is known to cross the placenta so we hypothesized that it would be secreted into milk (47).

We chose this indirect method of drug delivery because daily injection of ROSI would cause excessive stress to the dams/litters and worsen pup mortality. Taken together the decreased stress and manipulation of dams and litters were critical in developing this model.

Detection of rosiglitazone by mass spectrometry in lung tissue—We performed mass spectrometry analyses to detect rosiglitazone in neonatal mouse lung tissue on P13 to verify that the drug delivered in chow to the dams crossed through the milk and accumulated in neonatal lung tissue. We also tested lung tissue on P41 to verify that that weaned mice fed the impregnated chow also maintained a level of drug in their lung tissue (Supplemental Table 1).

Chemicals and Reagents: Rosiglitazone tablets were obtained from GlaxoSmith Kline as Avandia. HPLC grade methanol, HPLC grade acetonitrile, 200 proof ethanol, glacial acetic acid, formic acid, and ammonium hydroxide were obtained from Fisher Scientific (Fair Lawn, NJ). HPLC grade water was obtained from Burdick and Jackson (Muskegon, MI). Testosterone-d2 was obtained from Cambridge Isotopes (Andover, MA).

Extraction of Rosiglitazone from Tablets: 8 mg Rosiglitazone tablets were crushed into a fine powder with a mortar and pestle. 170 mg of crushed pill were added to 5 ml of 200 proof ethanol and extracted by vortexing for 15 seconds, and allowing to sit at room temperature for 30 minutes, vortexing for 15 seconds every 10 minutes. The extract was then centrifuged at 3200 RPM at 4°C for 10 minutes. The supernatant was removed and transferred to a 15 ml falcon tube. Concentration of Rosiglitazone at this point is 0.9 mg/ml.

Purification of Rosiglitazone by HPLC: Reverse phase HPLC was carried out on an Agilent 1200 series HPLC with a quaternary pump, diode array detector and fraction collector (Agilent Technologies, Santa Clara, CA). The column was an Agilent XDB-C18 50 mm × 4.6mm 1.8um. Buffer A was 0.1% formic acid in HPLC water and Buffer B was 0.1% formic acid in 9:1 acetonitrile:water. The HPLC program was a linear gradient of 3% B to 100% B over 20 minutes at 1.0ml/minute. 2 ul of the Rosiglitazone extract was injected and the peak eluting at 7.5 minutes was collected. 4 at 2ul aliquots were injected and collected. The acetonitrile was dried off in a vacuum centrifuge, and the remaining aqueous portion was frozen at -80°C, and then lyophilized until completed dry. The purified, dried extract was then reconstituted with HPLC methanol to give a final concentration of 10 ug/ml. This standard was then used for method optimization, instrument calibration and spiking solution.

Preparation of mouse lung for HPLC/MS/MS analysis: Lung tissue was isolated from mice as described on P13 or P41 and snap frozen in liquid nitrogen. Tissue was homogenized by grinding with a mortal and pestle. A predetermined aliquot of homogenized lung tissue was placed into a 1.5 ml microcentrifuge tube. 20 ul of internal standard solution (10 ng/ml testosterone-d2 in methanol-Testosterone-d2 was chosen from the available standards due to its similar molecular weight and similar chromatographic and ionization characteristics) was added to ~100-200 mg of tissue along with 1.0 ml of HPLC methanol. The sample was vortexed for 30 seconds and then placed into a -20°C freezer for 30 minutes with a 10 second vortex every 10 minutes. The sample was then centrifuged at 14K rpm for 10 minutes at 4°C. The supernatant was removed and then transferred to a new 1.5 ml microcentrifuge tube and dried in a vacuum centrifuge. The sample was then reconstituted with 200 uL of HPLC methanol and centrifuged at 14K rpm for 10 minutes before HPLC/MS/MS analysis. 10 uL of this extract was injected into the HPLC/MS/MS system.

Analysis of Rosiglitazone by HPLC/MS/MS: The HPLC/MS/MS system consisted of an Agilent 1200 series HPLC with a binary pump for the analytical column and a quaternary pump for the enrichment column, interfaced with a 6410 triple quadrupole mass spectrometer. The enrichment column was an Agilent Eclipse plus C8 12.5mm × 4.6mm 5um, and the analytical column was an Agilent XDB-C18 50mm × 2.1mm 1.8um. Buffer A was 0.02% acetic acid in water adjusted to pH 5.6 with 0.0072% ammonium hydroxide. Buffer B was 0.02% acetic acid with 0.0072% ammonium hydroxide in HPLC methanol. The quaternary pump used for sample enrichment was operated with the following gradient: 25%B for 0.5 minutes at 4 ml/min, decrease to 0.1 ml/min at 0.51 minutes for 3.49 minutes, increase %B from 25 to 100 and flow from 0.1 to 4 ml/min from 4 to 4.01 minutes, hold from 4.01 to 5 minutes, decrease %B from 100 to 25 from 5 to 5.01 minutes, hold at 25%B at 4 ml/min from 5.01 to 6 minutes. The binary pump used for the analytical column and separation of Rosiglitazone was isocratic at 80%B at 0.15 ms/min. The column-switching valve switched the binary pump to backflush the enrichment column and elute the Rosiglitazone onto the analytical column at 1 minutes for 3 minutes before switching back to the starting position.

Optimal mass spectrometer ionization conditions were determined by infusion of 10ng/ml Rosiglitazone in 20% buffer A and 80% buffer B at 150 uL/min. The mass spectrometer was

operated in the positive electrospray mode with a nitrogen drying gas temperature of 300°C at 10 L/min, a nebulizer pressure of 15 psi and a capillary voltage of 4000v. The fragmentor voltage was set at 115v and the collision energy at 27v. Data was collected in multiple reaction monitoring (MRM) mode to monitor the transition for Rosiglitazone at 358>135 Da and the testosterone-d2 internal standard at 291>111 Da.

Eight calibration standards of Rosiglitazone in HPLC methanol were analyzed in duplicate in a concentration range of 100 pg/ml to 500 ng/ml, using testosterone-d2 as an internal standard. Calibration curves were constructed using Agilent Masshunter Quantitative Analysis software. The equation for the calibration curve was y=41.778*x+0.1493 with a correlation coefficient (Rˆ2) of 0.9988. The concentration of Rosiglitazone in the tissue samples was calculated using this equation followed by multiplication of the result by the sample weight in grams. Results are expressed in pg/g.

Histological Analyses

Animals were euthanized with an overdose of inhaled isoflourane by a catheter placed in the trachea. The lungs were then perfused, fixed with buffered formalin under constant pressure 20cm H_2O for 45 min – 1 hour embedded and sectioned. Sections were analyzed by counting alveoli and vessels in 6 fields per section as previously reported (19). Briefly, ten high-powered fields were used for alveoli counting per animal (n=10 per group). Factor VIII-positive vessels were also counted in this manner to determine vessel density (not shown). PPAR-(, Ki67 (proliferation), cleaved caspase 3 (CC3; apoptosis) and alpha-smooth muscle actin (α-SMA; smooth muscle) were localized in paraffin embedded tissue sections using standard antibody staining technique recommended in the manufacturers' protocols (Santa Cruz Biotechnology, sc7273; Lab Vision Corporation NeoMarkers cat.#RM-9106.; Cleaved Caspase-3 (Asp175) Antibody Cell Signaling Technology #9661; DAKO 1A1). The qualitative colorimetric observations of α-SMA immunostaining with peroxidase substrate diaminobenzidine (DAB; Vector Labs Burlingame, CA) detection were confirmed by fluorescent staining.

Collagen deposition was analyzed using 2 staining techniques: Movat's pentachrome and Carstair's to verify results. Picosirius Red extraction was used to quantitate collagen relative to noncollagenous tissue. Picrosirius red staining was performed to detect and quantify collagen. Tissue sections were deparaffinized and incubated with 0.1% Sirius red / 0.1% fast green FCF (EM services, Hatfield PA) in picric acid for 30 minutes in the dark and rinsed with distilled water. Stain was extracted from tissue by the addition of equal volumes of methanol/0.1N sodium hydroxide. The eluate was diluted in distilled water and read using a spectrophotometer at 540 and 605 nm. The amount of noncollagenous protein was calculated by dividing the absorbance at 605nm by the lung fast green equivalence 2.22. The amount of collagenous protein was calculated from the absorbance at 540nm by subtracting 29% of the absorbance at 605nm and dividing by the Sirius red equivalence 36.3 (23).

Western blot was performed using frozen lung tissue samples, cut into small pieces and homogenized in lysis buffer and centrifuged (31). Equal amounts of protein (10ug) from the supernatant were loaded onto 16% Tris-Glycine gels for electrophoresis. Proteins were transferred to PVDF membrane, blocked with 5% nonfat milk, incubated with primary antibody (PPARγ-sc-7273; Santa Cruz Biotechnology) and then incubated with secondary antibody. A chemiluminescence system (ECL Plus, Amersham International) was used to generate autoradiographs of the membranes and densitometry was performed to quantify the luminescence signal (Adobe Photoshop; 31). Equal protein loading was confirmed by beta actin (Sigma A5441) immunostaining on the same blot. Six individual lung samples per group from independent experiments were analyzed on two separate analyses (n=6).

Affymetrix arrays and Array Analysis

Array analyses were conducted and analyzed as previously described (31). Briefly, RNA for analysis consisted of pooled samples from two or three different animals. Samples were prepared for Affymetricx arrays as previously described using standard techniques. Mouse genome 430 2.0 microarrays (Affymetrix, Foster City, CA) were hybridized with 20mg of cRNA and processed according to the manufacturers protocol. Affymetric Cel files were loaded into dChip 2005 array analysis software because the dChip algorithm is capable of detecting significant differences and low signal strengths. Signal strength from arrays were normalized to the median array, and expression levels were determined using the perfect match/mismatch algorithm. Gene ontology was determined using the Classify Genes tool within dChip, with gene ontology files downloaded from the Gene Ontology Consortium (HYPERLINK “http://www.geneontology.org/”www.geneontology.org). To avoid false negatives we set very loose definitions for changed genes as previously described and determined statistically overrepresented gene ontology groups at a high stringency ($P < 0.001$) within the genes called as differentially regulated. By this method, the number of gene ontology groups produced by chance should be close to 0. Statistical significance for overrepresented gene ontology groups was determined by the one-sample z-test, incorporated into the dChip software.

Measurement of pulmonary function and airway responsiveness

Pulmonary function was measured by a low frequency forced oscillation technique to obtain impedance data which included tissue damping, tissue elastance and lung resistance (8 33 35 40). Mice were exposed to hyperoxia from P0-P10 and treated with ROSI until P30. From P30 to P55 mice were maintained on standard chow. Airway responsiveness was monitored on P55 through changes in lung resistance (RL) and dynamic compliance (Cdyn) in response to inhaled methacholine (MCh) in anesthetized, tracheostomized mice as described by Takeda et al. (33). Ventilation was achieved at 160 breaths/min and a tidal volume of 0.15 ml with a positive end-expiratory pressure of 2-4 cm H_2O. Flow was measured by digital differentiation of the volume signal. Lung resistance (RL) and dynamic compliance (Cdyn) will be continuously computed (Labview, National Instruments, TX) by fitting flow, volume, and pressure to an equation of motion (33 35). Aerosolized MCh was administered through bypass tubing via an ultrasonic nebulizer (model 5500D, DeVilbiss, Somerset, PA) placed between the expiratory port of the ventilator and the four-way connector. Aerosolized MCh was administered for 10 seconds with a tidal volume of 0.45 ml and frequency of 60 BPM using another ventilator (SN-480-7). The data of RL and Cdyn were continuously collected for up to three minutes and maximum values were taken.

Statistical Analysis

All experiments followed a randomized block design with the use of cells from a least two different animals. Assays were completed from at least 4 independent experiments consisting of 2-6 replicates in each. Data were expressed as means ± standard error, and significance between groups was determined by one-way ANOVA or student's t-test with Tukey adjustment, using the statistical software package JMP5 (SAS Institute, Cary, NC). A 2-way ANOVA was performed to detect significance of *in vivo* analyses. Statistical significance was set at $P<0.05$. alpha=0.05. *denotes significance for $p < 0.05$. ** for $p < 0.01$, *** for $p<0.001$.

Results

PPAR-γ Expression Decreases Following Neonatal Exposure to Hyperoxia

We have previously reported that exposure of newborn mice to chronic hyperoxia resulted in hypoalveolarization and decreased vessel density, which persisted into adulthood (19). To evaluate the contribution of PPAR-γ to this process, we first analyzed the change in protein localization and expression of PPAR-γ in the developing lungs following a 10 day exposure to chronic HE. In control RA mice at P13 and P41, PPAR-*γ* was immunolocalized in the lungs to the epithelium, endothelium and tissue macrophages, similar to previous reports (Figure 1A-D;11 17 22 28 29). At P13, following the hyperoxic exposure, the expression of PPAR-*γ* by immunohistochemistry was visibly decreased. As an internal positive control, though PPAR-γ was minimally expressed in the lung of P13 HE animals, it remained abundant in the adjacent fatty tissue from these mice (Supplemental Figure1A&B). To evaluate nuclear localization of PPAR-γ, staining was repeated with immunofluorescence which showed nuclear PPAR-γ present in parenchymal cells following RA exposure, likely within macrophages and lipofibroblasts adjacent to alveolar type II cells. In contrast, no significant PPAR-γ staining was detected in the HE group (Figure 2A&B). Treatment with the PPAR-γ agonist, ROSI, in combination with HE did not significantly increase PPAR-γ protein expression or levels in the epithelial, endothelial or parenchymal cells (Figures 1E,F; 2C;3). By P41 PPAR-γ was expressed in the endothelium and airway epithelium of RA, HE and HE+ROSI mice with no observable difference between groups (not shown). Findings by immunolocalization were confirmed by immunoblot of lung tissue. At P13, protein levels of PPAR-*γ* were significantly decreased in the lung following HE ($p<0.007$) and HE+ROSI ($p<0.015$; Figure 3A). PPAR-γ, expression was restored by P41, with similar expression levels in RA, HE and HE + ROSI lungs (Figure 3B). Multiple isoforms of PPAR-γ were detected. These multiple isoforms have no reported distinct functions and result from the expression of PPAR-γ from two overlapping promoters (16,21).

Treatment with the PPARγ Agonist Rosiglitazone Rescues Neonatal Lung Structure following Chronic Hyperoxic Exposure

On P13, following exposure to hyperoxia, minimal (no measurable) changes in alveolarization were detected compared to RA (Figure 4A,C,E,G). However, by P41, lungs from HE mice exhibited marked hypoalveolarization (Figure 4B,F) with a decrease in alveolar density ($p<0.001$) compared to RA mice (Figure 5A). In addition, microvascular density per field of lung tissue was decreased in HE mice ($p<0.01$) (Figure 5B). Treatment with the PPAR-γ agonist ROSI restored both alveolarization and vascular development at P41 (Figure 4H). Alveolar density and microvascular density in HE + ROSI were similar to RA and significantly increased compared to HE alone ($p<0.001$ and $p<0.01$ vs HE respectively) (Figure 5 A,B). ROSI treatment during RA exposure had no effect on alveolar or microvascular densities (Figures 4C,D &5). ROSI did not protect against the growth delay at P13 observed in the HE mice, shown by lower body weights in HE and HE + ROSI compared with RA (Figure 5C). No difference in body weight was observed between groups by P41.

We measured ROSI in neonatal lung tissue by mass spectroscopy to verify that ROSI crossed into the dams' milk and subsequently accumulated in neonatal lung tissue at P13 and that weaned mice fed the impregnated chow also maintained a level of drug in their lung tissue. We detected ROSI in lung tissue of both nursing (P13) and weaned mice (P41) (n=2 for each time-point to confirm reproducibility). Using a ROSI standard (AVANDIA, Glaxo Smith Kline) we determined the mean ROSI concentration within homogenized lung tissue to be 90.7 pg/g on P13 and 7074.0 pg/g on P41 (Supplemental Table 1).

Changes in Lung Gene Expression in Hyperoxic Exposed Mice

To determine effects of HE and HE+ROSI on global expression of RNA transcripts in lung tissue relative to RA, we compared gene expression levels using the Affymetrix MOE430A arrays. In addition to changes in ROSI target genes (Table 1;49) we found a large number of genes changed following HE and HE+ROSI at P13 compared with RA controls. Both groups had changes in numbers of cell cycle, angiogenesis, developmental, matrix-related, and muscle development or contraction-related genes. Examples selected from these groups are listed in Table 2. In general pro-cell-cycle genes (cyclins A2,B1,2,D2,E2,T1,2, CDK4, CDK6) were decreased and cell cycle inhibitors were increased (p21) following HE.

Changes in lung transcript levels resulting from ROSI treatment during HE relative to HE alone were analyzed by comparing the changes found in the HE-pooled chips to those in the HR-pooled chips and again used classification into gene ontology groups to establish significance. HE+ROSI mice had a significant degree of change in the ontology groups including blood vessel morphogenesis, muscle differentiation/contraction, pattern specification and morphogenesis and response to stimuli-related genes. A list of examples is shown in Table 3. Array analysis indicated that there was a significant ROSI-dependent downregulation of pro-smooth muscle/myofibroblast differentiation and contraction markers, including WISP1 and pro-collagen mRNA.

PPARγ Agonist Decreased Myofibroblast Accumulation during Postnatal Lung Development

In order to examine how loss of PPAR-γ signaling following chronic hyperoxic exposure could lead to protective changes in pulmonary structure and function, we analyzed potential targets of the agonist related to myofibroblast differentiation and collagen production identified by the gene array. HE resulted in myofibroblast accumulation, detected by α-SMA immunostaining, within the lung parenchyma relative to RA on P13 (Figure 6 D-F). The increase in α-SMA immunostaining was attenuated in the ROSI+HE group (Figure 6G-I). No change in airway α-SMA expression or thickness was detected on P13 or 41 in response to HE (Figure 7). On P41 there was no evidence for chronic inflammation associated with airway / arteriolar structures. No apoptosis was detected by cleaved caspase 3 immunostaining between groups on P13 or P41 (not shown).

Increased extracellular matrix production by myofibroblasts can decrease lung function (9 11 25-27 34). We therefore stained for collagen by two methods, Carstairs and Movat's Pentachrome (not shown) staining, to evaluate collagen deposition. By both methods, collagen was visibly associated with airway – arteriole vessel structures in the lung tissues (Figure 8A-F) however no qualitative differences were detected between groups on P13 or P41. Quantification of total collagenous protein as a ratio to non-collagenous protein was performed using Sirius red staining and extraction (23). No significant difference in these ratios between groups was detected on P13 or P41 (Figure 8G). No clear change in distribution of collagen was noted but a developmental increase in collagen accumulation was detected ($p<0.01$; 9 34) from P13 to P41.

Rosiglitazone Treatment Attenuates the Development of Airway Hyper-responsiveness following HE

Another important sequelae of CLD is the development of airway hyperresponsiveness (AHR) (8 10 14 41). Another important sequelae of CLD is the development of airway hyperresponsiveness (AHR), which can be mediated by changes in myofibroblasts, smooth muscle function or subtle alterations in the pulmonary immune response (8 10 14 41). As we did not see changes in collagen production associated with increased myofibroblasts, or increased smooth muscle thickening, we analyzed the pulmonary function and airway

responsiveness in adult mice following neonatal exposure to RA or HE. Airway responsiveness was analyzed following inhalation of MCh and measurements of both airway resistance and dynamic compliance were compared to the baseline response to saline (Figure 9A&B). RA and RA+ROSI had similar baseline changes in airway resistance to MCh challenge. However, mice exposed to neonatal hyperoxia (HE) showed significantly increased airway responsiveness to MCh than the comparable control group (RA) ($p<0.01$). HE+ROSI treatment significantly decreased airway responsiveness relative to the HE group ($p<0.05$), to a level similar to RA treatment. Despite significant changes with MCH challenges, no significant differences were noted in the tissue damping, tissue elastance and lung resistance between groups (Table 4).

Discussion

Because loss of PPAR–γ in the rodent airway epithelium disrupts development resulting in loss of alveolar surface area (28 29) we sought to enhance PPAR-γ activity with the agonist rosiglitazone to acertain its importance in this process. We previously reported that newborn mice exposed at birth to moderate hyperoxia developed morphologic changes and AHR characteristic of human CLD of infancy (also known as bronchopulmonary dysplasia). Here we extended our previous report by additionally measuring and confirming the presence of AHR, which persists into adulthood. This is a highly relevant animal model as it mirrors the human condition in which infants born prematurely are at risk for reactive airways disease as children and adults. We have begun to evaluate the mechanisms responsible for late AHR following CLD by evaluating the role for PPAR-γ in this process. We now report that PPAR-γ expression is decreased in hyperoxia-exposed newborn mice. Furthermore, treatment during neonatal hyperoxic exposure with the PPAR-γ receptor agonist, ROSI, prevented the development of CLD. ROSI treatment during HE restored alveolar and microvascular density and decreased myofibroblast accumulation to RA control levels. Importantly, in addition to improving lung alveolar and vascular development, ROSI treatment also prevented the subsequent development of AHR. These findings provide new insight into the role of PPAR-γ in the development of CLD and AHR.

There is a strong rationale for examining the role of PPAR-γ in the developing lung and testing its role in the development of chronic lung disease. PPAR-γ plays a regulatory role in the fetal to newborn transition on both the maternal side by suppressing the production of milk containing elevated levels of inflammatory lipids (38) and in the developing lung, where its expression increases just prior to birth (28 29). We found an increase in PPAR-γ expression in the developing lung, which was reduced by early exposure to chronic hyperoxia. Its localization in the lung was similar to prior reports showing both endothelial, epithelial and macrophage expression (28 29). We also detected nuclear PPAR-γ expression adjacent to type II epithelial structures which may be indicative of lipofibroblasts. Interestingly, the loss of PPAR-γ in the afore mentioned cell types precedes the subsequent change in both alveolar and vascular development. Our study was unique as well in that we administered ROSI to newborn mice by treating the dams and, once weaned, continued feeding the weanling mice with ROSI impregnated chow. We demonstrated by mass spectroscopy that both methods delivered drug to the lungs of the offspring.

Our first key observation was that treatment with the PPAR-γ agonist, ROSI attenuated both hypoalveolarization and loss of microvascular density, which developed in adult mice (P41) after exposure to moderate hyperoxia as newborns. These studies extend the observation in a model of acute hyperoxic exposure to high concentrations of oxygen (95% oxygen) for 24-hours in which the receptor agonist, ROSI, protected alveolarization (25-27 36) as well as postnatal angiogenesis (37 39). ROSI or other PPAR-γ agonists have been shown to protect against a variety of other lung diseases including ventilator induced lung injury and

bleomycin induced pulmonary fibrosis (17 22). While the data surrounding the effects of ROSI and PPAR-γ signaling as pro or anti-angiogenic are controversial (46) our array data suggests a pro-angiogenic response of ROSI in the setting of hyperoxia compared with HE alone via the increased expression of endoglin, thrombospondin, ephrins, VEGFR1 (Flt-1) and endothelial differentiation sphingolipid G-protein-coupled receptor 1 ($S1P_1$).

ROSI protected against the effects of HE despite a lack of increase in PPAR-γ protein expression. These data suggest that PPAR-γ activity is regulated at the post-translational level and the existing receptor levels, though decreased, are able to respond to agonist stimulation. Other studies support this possibility. Functional protein is essential for PPAR-γ signaling, as targeted deletion of PPAR-γ in epithelium during postnatal lung development results in abnormal lung structure and function (28). The ability of cells to respond to PPAR-γ agonists in the presence of decreased levels of PPAR-γ protein have been reported for lung fibroblasts, non-small cell lung cancer cells and endothelial cells (1 22 43). In fibroblast lung cell isolates from adult pulmonary fibrosis patients, PPAR-γ agonists inhibited fibroblast and myofibroblast differentiation, proliferation and collagen deposition without increasing PPAR-γ protein levels (22). There are a number of potential mechanisms which may account for changes in PPAR-γ function following ligand binding. Agonist stimulation can change expression or binding affinities of co-activators or repressors (1 43). The function of PPAR-γ proteins is regulated by the conformation of the ligand binding domain, influenced by co-activator or inhibitor proteins as well as proteins required for heterodimer formation and DNA binding activity (4 44). We did observe an increase in retinoic acid receptor–alpha (RARα) message, a co-activator for PPAR-γ, following hyperoxia with ROSI treatment. These functional differences mediated by protein-protein interactions provide a basis for future studies to more completely understand the mechanism of action by which PPAR-γ agonists protect.

Our array analysis indicated that there was a significant downregulation of pro-smooth muscle/myofibroblast differentiation and contraction markers with ROSI treatment. These findings were further confirmed by histochemical analyses of αSMA expression in the neonatal lungs. One potential mechanism by which ROSI can protect lung development and maturation is by preventing abnormal differentiation of multipotent progenitors. The regulation of lipofibroblast versus myofibroblast differentiation during lung development leading to a change in lung structure and function may prove to be the most relevant (25-27 36). Lipofibroblasts are located in the alveolar interstitium and are recognizable by lipid droplets. During alveolar development they participate in the synthesis of extracellular matrix structural proteins, such as collagen and elastin, induce epithelial type II (TII) cell differentiation and function as an accessory cell to the type II pneumocyte in the synthesis of surfactant (50). The loss of lipofibroblasts, appearance of myofibroblasts and subsequent proliferation are key events in the development of CLD. In addition, ROSI has also been shown to facilitate the differentiation of multipotent progenitors toward an endothelial cell type over an α-SMA positive myofibroblast or smooth muscle cell type *in vivo* to prevent vascular remodeling (39). It is possible the same is true for multipotent epithelial progenitors. Increased α-SMA positive phenotypes can parallel a loss of PPAR-(with corresponding decreases in epithelial differentiation and increased contractile myofibroblasts (6 25-27). PPAR-γ signaling also decreases the metastatic epithelial-mesenchymal transition (EMT) in lung cancer cells by promoting a more differentiated epithelial phenotype (43). PPAR-γ dependent mechanisms of ROSI protection against EMT and subsequent have been demonstrated using *in vitro* studies in which treatment inhibited TGFβ mediated myofibrobalst differentiation and collagen secretion (11). In addition, the administration of ROSI following the inflammatory phase of bleomycin injury in mice suggests that the protective effect is mediated through the regulation of myofibroblast differentiation and to a lesser degree modulation of the inflammatory response (22).

Hyperoxic exposed mice have an abnormal response to methacholine as adults, similar to the clinical scenario often seen when former preterm babies exhibit challenges with airway mechanics when faced with illness later in life. In addition, the development of AHR, manifested by changes in lung resistance or dynamic compliance in response to inhaled Mch, was attenuated in adult mice that received ROSI treatment during neonatal HE. These observations suggest that there may be a specific temporal requirement or window for PPAR-γ signaling in response to hyperoxia to regulate inflammation, proliferation and / or cell differentiation, which have long-term effects. The increase in TGFβ2 message on P13 in lung tissue following hyperoxia and its 4-fold decreased in the ROSI treated group is a significant finding because it represents a risk factor for airway remodeling and asthma (39). In other rodent models of lung injury ROSI exhibits anti-inflammatory effects on the epithelial cells of the air passages, alveolar macrophages and neutrophils by decreasing both recruitment and release of inflammatory cytokines in the lung (20 24 32). Ideally, the minimum window to achieve these effects with ROSI treatment needs to be determined to avoid detrimental side effects such as potential changes in cardiac and pulmonary function. Further evaluation of the possible adverse effects of ROSI+HE on lung function may be warranted based on the Cst approaching significance.

To date the origin of AHR responses in humans is unclear but hypothesized to be linked to genetics, lung injury or abnormal airway development including remodeling (45). In the face of AHR there we did not find significant evidence of airway remodeling including thickening of airway smooth muscle detected by α-SMA staining. There was a lack of goblet cell hyperplasia as well as evidence of substantial chronic inflammation or collagen accumulation typically associated with adult models of chronic allergic asthma (5 33 42). The lack of gross inflammatory changes in adult mice exposed to hyperoxia (100% 4 days) as neonates has previously been demonstrated (24). However, a difference in the immune response has been reported to present upon a secondary inflammatory challenge. Rodent models of chronic asthma exhibit airway remodeling due to presence of chronic inflammation. The lack of these indications of AHR in the adult lungs in the HE+ROSI group suggests developmental changes in contractile cell phenotype and function or subtle alterations in the immune response mediated by PPARγ which persist into adulthood. The absence of fixed airway obstruction in this model allows the study of AHR in the context of CLD.

The mechanism by which ROSI action, either directly or indirectly, promotes normal alveolarization and lung function through modulation of postnatal components of the immune response remains to be determined. Changes in inflammatory cell repertoire and cytokines during and following hyperoxic exposure of the neonatal mice were indicated by the array analyses and will be the focus of future studies. The contribution of off target effects of ROSI may also provide insight into its beneficial effects. Our data suggests that PPAR-γ signaling could be required in at least two related activities in our study, as an anti-inflammatory mediator and anti-myofibroblast differentiation factor. In addition, ROSI is known to increase adipogenesis, which may influence the nutrients present in dams' milk. While ROSI protected against the changes in lung structure and function there was not significant effect on pup weight between the hyperoxia alone and HE+ROSI groups. Taken together with previously published data, these results suggest that the protective effects on lung structure observed were due to ROSI treatment and PPAR signaling in the neonatal lung tissue.

It is critical that early treatment with ROSI during hyperoxic exposure attenuated experimental CLD and improved the long-term sequelae, AHR. Taken together PPARγ signaling appears to be protective of early proliferation in lung and decreased myofibroblast differentiation, perhaps sustaining normal development. These data suggest multiple

mechanisms by which PPAR-γ signaling regulates the development of lung structure and function. Following HE and decreased expression of PPAR-γ protein, cell proliferation decreased and α-SMA expression increased in the absence of significant remodeling by collagen deposition or marked changes in inflammation. Additionally, AHR was increased. HE with ROSI treatment increased cell proliferation and reduced α-SMA expression resulting in increased septation and decreased AHR. ROSI mediated these protective effects in the absence of apparent increased PPAR-γ protein expression. The elucidation of the subtle changes in cell phenotype, differentiation and inflammation which result in AHR has to be addressed and will be a useful tool in the development of therapies for AHR, one of the most common long-term problems associated with preterm birth.

Supplementary Material

Refer to Web version on PubMed Central for supplementary material.

Acknowledgments

This work was funded by grants to S.M. Majka from the American Heart Association (SDG-0335052N), the Denver Childrens Hospital Pilot Award and the American Physiological Society Giles Filley Award. Additional support for collaborating investigators was provided by E. Gelfand NIH 36577, HL-61005, EPA R825702; D. Klemm P01-HL014985 and E. Grayck RO1-HL 086680.

References

1. Akaike M, Che W, Marmarosh N, Ohta S, Osawa M, Ding B, Berk BC, Yan C, Abe J. The Hinge-Helix 1 Region of Peroxisome Proliferator-Activated Receptor 1 (PPAR1) Mediates Interaction with Extracellular Signal-Regulated Kinase 5 and PPAR1 Transcriptional Activation: Involvement in Flow-Induced PPAR Activation in Endothelial Cells. Molecular and Cellular Biology. 2004; 24:8691–8704. [PubMed: 15367687]
2. Ameshima S, Golpon H, Cool CD, Chan D, Vandivier RW, Gardai SJ, Wick M, Nemenoff RA, Geraci MF, Voelkel NF. Peroxisome Proliferator-Activated Receptor Gamma (PPAR) Expression Is Decreased in Pulmonary Hypertension and Affects Endothelial Cell Growth. Circulation Research. 2003; 92:1162. [PubMed: 12714563]
3. Belvisi MG, Hele DJ. Peroxisome Proliferator-Activated Receptors as Novel Targets in Lung Disease. Chest. 2008; 134:152–157. [PubMed: 18628217]
4. Berger J, Moller DE. The mechanisms or action of PPARS. Annu Rev Med. 2002; 53:409–435. [PubMed: 11818483]
5. Birrell MA, Patel HJ, McCluskie K, Wong S, Leonard T, Yacoub MH, Belvisi MG. PPAR- agonists as therapy for diseases involving airway neutrophilia. Eur Respir J. 2004; 24:18–23. [PubMed: 15293600]
6. Boros LG, Torday JS, Lee WP, Rehan VK. Oxygen-induced metabolic changes and transdifferentiation in immature fetal rat lung lipofibroblasts. Molecular Genetics and Metabolism. 2000; 77:230–236. [PubMed: 12409271]
7. Bourbon J, Boucherat O, Chailley-Heu B, Delacourt C. Control Mechanisms of Lung Alveolar Development and Their Disorders in Bronchopulmonary Dysplasia. Pediatr Res. 2005; 57:38R–46R.
8. Bozanich EM, Collins RA, Thamrin C, Hantos Z, Sly PD, Turner DJ. Developmental changes in airway and tissue mechanics in mice. J Appl Physiol. 2005; 99:108–113. [PubMed: 15817717]
9. Bradley KH, McConnell SD, Crystal RG. Lung Collagen Composition and Synthesis. J Biol Chem. 1974; 249:2674–2683. [PubMed: 4364025]
10. Brooks AM, Byrd RS, Weitzman M, Auinger P, McBride JT. Impact of Low Birth Weight on Early Childhood Asthma in the United States. Arch Pediatr Adolesc Med. 2001; 155:401–406. [PubMed: 11231809]
11. Burgess HA, Daugherty LE, Thatcher TH, Lakatos HF, Ray DM, Redeonnet M, Phipps RP, Sime PJ. PPARγ agonists inhibit TGF-β induced pulmonary myofibroblast differentiation and collagen

production: implications for therapy of lung fibrosis. Am J Physiol Lung Cell Mol Physiol. 2005; 288:L1146–1153. [PubMed: 15734787]

12. Crossno JT Jr, Majka SM, Grazia T, Gill RG, Klemm DJ. Rosiglitazone promotes development of a novel adipocyte population from bone marrow-derived circulating progenitor cells. J Clin Invest. 2006; 116:3220–3228. [PubMed: 17143331]
13. Cuzzocrea S, Pisano B, Dugo L, Ianaro A, Maffi P, Patel NS, Di Paola R, Ialenti A, Genovese T, Chatterjee P, Di Rosa M, Caputi AP, Thiemermann C. Rosiglitazone, a ligand of the peroxisome proliferator-activated receptor-γ, reduces acute inflammation. European Journal of Pharmacology. 2004; 483:79–93. [PubMed: 14709329]
14. Eber E, Zach MS. Long term sequelae of bronchopulmonary dysplasia (chronic lung disease of infancy). Thorax. 2001; 56:317–323. [PubMed: 11254826]
15. Ghosh AK, Bhattacharyya S, Lakos G, Chen S, Mori Y, Varga J. Disruption of Transforming Growth Factor β Signaling and Profibrotic Responses in Normal Skin Fibroblasts by peroxisome Proliferator-Activated Receptor γ. Arthritis & Rheumatism. 2004; 50:1305–1318. [PubMed: 15077315]
16. Han J, Hajjar DP, Zhou X, Gotto AM Jr, Nicholson AC. Regulation of PPARg-Mediated Gene Expression: A New Mechanism of Action for High Density Lipoprotein. J Biol Chem. 2002; 277:23582–23586. [PubMed: 11953427]
17. Hoetzel A, Dolinay T, Vallbracht S, Zhang Y, Kim HP, Ifedigbo E, Alber S, Kaynar AM, Schmidt R, Ryter SW, Choi AMK. Carbon Monoxide Protects against Ventilator-induced Lung Injury via PPAR- and Inhibition of Egr-1. American Journal of Respiratory and Critical Care Medicine. 2008; 177:1223–1232. [PubMed: 18356564]
18. Hsueh WA, Jackson S, Law RE. Control of vascular Cell Proliferation and Migration by PPAR-γ. A new approach to the macrovascular complications of diabetes. Diabetes Care. 2001; 24:392–397. [PubMed: 11213897]
19. Irwin D, Helm K, Campbell N, Imamura M, Fagan K, Harral J, Carr M, Young KA, Klemm D, Gebb S, Dempsey EC, West J, Majka S. Hyperoxic Induced Changes in Pulmonary Lung Side Population of Progenitor populations. AJP:LCMP. 2007; 293:L941–51.
20. Liu D, Zeng BX, Zhang SH, Yao SL. Rosiglitazone, an agonist of peroxisome proliferators-activated receptor γ, reduces pulmonary inflammatory response in a rat model of endotoxemia. Inflamm Res. 2005; 54:464–470. [PubMed: 16307220]
21. Marx N, Bourcier T, Galina K, Libby P, Plutzky J. PPARγ Actitivation in Human Endothelial Cells Increases Plasminogen Activator Type-1 Expression PPARγ as a Potentional Mediator in Vascular Disease. Arterioscler Thromb Vasc Biol. 1999; 19:546–551. [PubMed: 10073956]
22. Milam JE, Keshamouni VG, Phan SH, Hu B, Gangireddy SR, Hogaboam CM, Standiford TJ, Thannickal VJ, Reddy RC. PAR-g agonists inhibit profibrotic phenotypes in human lung fibroblasts and bleomycin-induced pulmonary fibrosis. Am J Physiol Lung Cell Mol Physiol. 2008; 294:L891–L901. [PubMed: 18162602]
23. Nozik-Grayck E, Suliman HB, Majka SM, Albietz J, Van Rheen Z, Roush K, Stenmark KR. Lung EC-SOD Overexpression Attenuates Hypoxic Induction of Egr-1 and Chronic Hypoxic Pulmonary Vascular Remodeling. Am J Physiol Lung Cell Mol Physiol. 2008 ePUB. 10.1152/ajplung.90293
24. O'Reilly MA, Marr SH, Yee M, McGrath-Morrow SA, Lawrence BP. Neonatal Hyperoxia Enhances the Inflammatory Response in Adult Mice Infected With Influenza A Virus. Am J Respir Crit Care Med. 2008; 177:1103–1110. [PubMed: 18292469]
25. Rehan VK, Torday JS. Hyperoxia augments pulmonary lipofibroblast-to-myofibroblast transdifferentiation. Cell Biochemistry and Biophysics. 2003; 38:239–249. [PubMed: 12794266]
26. Rehan VK, Wang Y, Patel S, Santos J, Torday JS. Rosiglitazone, a Peroxisome Proliferator-Activated Receptor-γ Agonist, Prevents Hyperoxia-induced Neonatal Rat Lung Injury In Vivo. Pediatric Pulmonology. 2006; 41:558–569. [PubMed: 16617452]
27. Rehan VK, Sugano S, Wang Y, Santos Romero S, Dasgupta C, Keane MP, Stahlman MT, Torday JS. Evidence for the presence of lipofibroblasts in human lung. Experimental Lung Research. 2006; 32:379–393. [PubMed: 17090478]

28. Simon DW, Arikan MC, Srisuma S, Bhattacharya S, Tsai LW, Ingenito EP, Gonzalez F, Shapiro SD, Mariani TJ. Epithelial cell PPAR contributes to normal lung maturation. The FASEB Journal. 2006; 20:1507–1509. [PubMed: 16720732]
29. Simon DM, Mariani TJ. Role of PPARs and Retinoid X Receptors in the Regulation of Lung Maturation and Development. Ped Res. 2007; 2007:91240.
30. Tachibana K, Kobayashi Y, Tanaka T, Tagami M, Sugiyama A, Katayama T, Ueda C, Yamasaki D, Ishimoto K, Sumitomo M, Uchiyama Y, Kohro T, Sakai J, Hamakubo T, Kodama T, Doi T. Gene expression profiling of potential peroxisome proliferator-activated receptor (PPAR) target genes in human hepatoblastoma cell lines inducibly expressing different PPAR isoforms. Nuclear Receptor. 2005; 3:3–7. [PubMed: 16197558]
31. Tada Y, Majka S, Carr M, Harral J, Crona D, Kuriyama T, West J. Molecular effects of loss of BMPR2 signaling in smooth muscle in a transgenic mouse model of PAH. Am J Physiol Lung Cell Mol Physiol. 2007; 292:L1556–L1563. [PubMed: 17369292]
32. Takata Y, Kitami Y, Yang Z, Nakamur M, Okura T, Hiwada K. Vascular Inflammation Is Negatively Autoregulated by Interaction Between CCAAT/Enhancer-Binding Protein-δ and Peroxisome Proliferator-Activated Receptor-γ. Circ Res. 2002; 91:427–433. [PubMed: 12215492]
33. Takeda K, Hamelmann E, Joetham A, Shultz LD, Larsen GL, Irvin CG, Gelfand EW. Development of Eosinophilic Airway Inflammation and Airway Hyperresponsiveness in Mast Cell-deficient Mice. J Exp Med. 1997; 186:449–454. [PubMed: 9236197]
34. Thibeault DW, Mabry SM, Ekekezie II, Zhang X, Truog WE. Collagen Scaffolding During Development and Its Deformation With Chronic Lung Disease. Pediatrics. 2003; 111:766–776. [PubMed: 12671110]
35. Tomioka S, Bates JHT, Irvin CG. Airway and tissue mechanics in a murine model of asthma: alveolar capsule vs. forced oscillations. J Appl Physiol. 2002; 93:263–270. [PubMed: 12070213]
36. Torday JS, Torres E, Rehan VK. The role of fibroblast transdifferentiation in lung epithelial cell proliferation, differentiation and repair in vitro. Ped Pulmonary and Molecular Medicine. 2003; 22:189–207.
37. Uno K, Merges CA, Grebe R, Lutty GA, Prow TW. Hyperoxia inhibits several critical aspects of vascular development. Dev Dyn. 2007; 236:981–90. [PubMed: 17366630]
38. Wan Y, Saghatelian A, Chong L, Zhang C, Cravatt BF, Evans RM. Maternal PPAR protects nursing neonates by suppressing the production of inflammatory milk. Genes & Development. 2007; 21:1895–1908. [PubMed: 17652179]
39. Wang C, Ciliberti N, Li S, Szmitko PE, Weisel RD, Fedak PWM, Al-Omran M, Cherng W, Li R, Stanford WL, Verma S. Rosiglitazone Facilitates Angiogenic Progenitor Cell Differentiation Toward Endothelial Lineage. Circulation. 2004; 109:1392–1400. [PubMed: 14993120]
40. Ward JE, Fernandes DJ, Taylor CC, Bonacci JV, Quan L, Stewart AG. The PPARγ ligand, rosiglitazone, reduces airways hyperresponsiveness in a murine model of allergen-induced inflammation. Pulmonary Pharmacology & Therapeutics. 2006; 19:39–46. [PubMed: 16286236]
41. Warner BB, Stuart LA, Papes RA, Wispé JR. Functional and pathological effects of prolonged hyperoxia in neonatal mice. Am J Physiol Lung Cell Mol Physiol. 1998; 275:L110–L117.
42. Wilder JA, Collie DS, Bice DE, Tesfaigzi Y, Lyons CR, Lipscomb MF. Ovalbumin aerosols induce airway hyperreactivity in naïve DO11.10 T cell receptor transgenic mice without pulmonary eosinophilia or OVA-specific antibody. Journal of Leukocyte Biology. 2001; 69:538–547. [PubMed: 11310839]
43. Winn RA, Van Scoyk M, Hammond M, Rodriguez K, Crossno JT, Heasley LE, Nemenoff RA. Antitumorigenic Effect of Wnt 7a and Fzd 9 in Non-small Cell Lung Cancer Cells Is Mediated through ERK-5-dependent Activation of Peroxisome Proliferator-activated Receptor. J Biol Chem. 2006; 281:26943–26950. [PubMed: 16835228]
44. Yu S, Reddy JK. Transcription coactivators for peroxisome proliferator-activated receptors. Biochim Biophys Acta. 2007; 1771:936–51. [PubMed: 17306620]
45. Baraldi E, Filippone M. Chronic Lung Disease after Premature Birth. NJEM. 2007; 357:1946–1955.
46. Margeli A, Kouraklis G, Theocharis S. Peroxisome Proliferator Activated Receptor-γ (PPAR-γ) Ligands and Angiogenesis. Angiogenesis. 2003; 6:165–169. [PubMed: 15041792]

47. Choi JS, Han JY, Ahn HK, Shin JS, Yang JH, Koong MK, Nava-Ocampo AA. Exposure to Rosiglitazone and Fluoxetine in the First Trimester of Pregnancy. Diabetes Care. 2006; 29:2176. [PubMed: 16936175]

48. Bry K, Whitsett JA, Lappalainen U. IL-1β Disrupts Postnatal Lung Morphogenesis in the Mouse. Am J Respir Cell Mol Biol. 2007; 36:32–42. [PubMed: 16888287]

49. Keen HL, Ryan MJ, Beyer A, Mathur S, Scheetz TE, Gackle BD, Faraci FM, Casavant TL, Sigmund CD. Gene Expression Profiling of Potential PPAR Target Genes in Mouse Aorta. Physiol Genomics. 2004; 18:33–42. [PubMed: 15054141]

50. McGowan SE, Torday JS. The Pulmonary Lipofibroblast (Lipid Interstitial Cell) and Its Contributions to Alveolar Development. Annual Review of Physiology. 1997; 59:43–62.

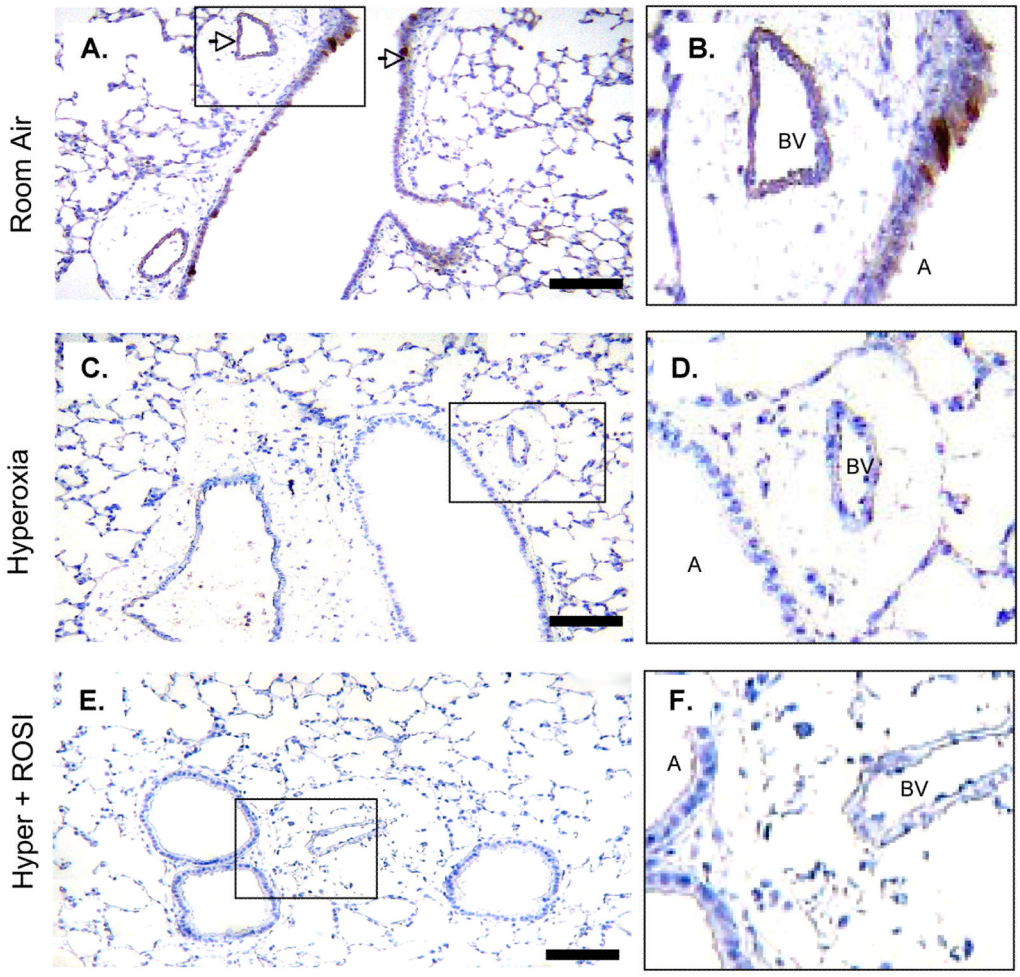

Figure 1. PPAR-γ Protein Localization is Significantly Altered in Lung Airway Epithelium and Arteriolar Structures Following Neonatal Hyperoxic Exposure

Immunostaining was performed to detect PPAR-γ expression at RA, in response to hyperoxic exposure and HE+ROSI. On P13 PPAR-γ protein expression was detected in the RA group airway epithelium and endothelium. Expression was decreased in the hyperoxic exposed and HE+ROSI groups. Representative images of immunostain of **A.** RA **B.** Hyperoxic exposed, **C.** HE+ROSI with DAB detection. PPARγ reactivity appeared brown and indicated by arrow. Scale bar=50uM. **B,D,F.** Respective enlargements of airway and arteriole from **A-C**.

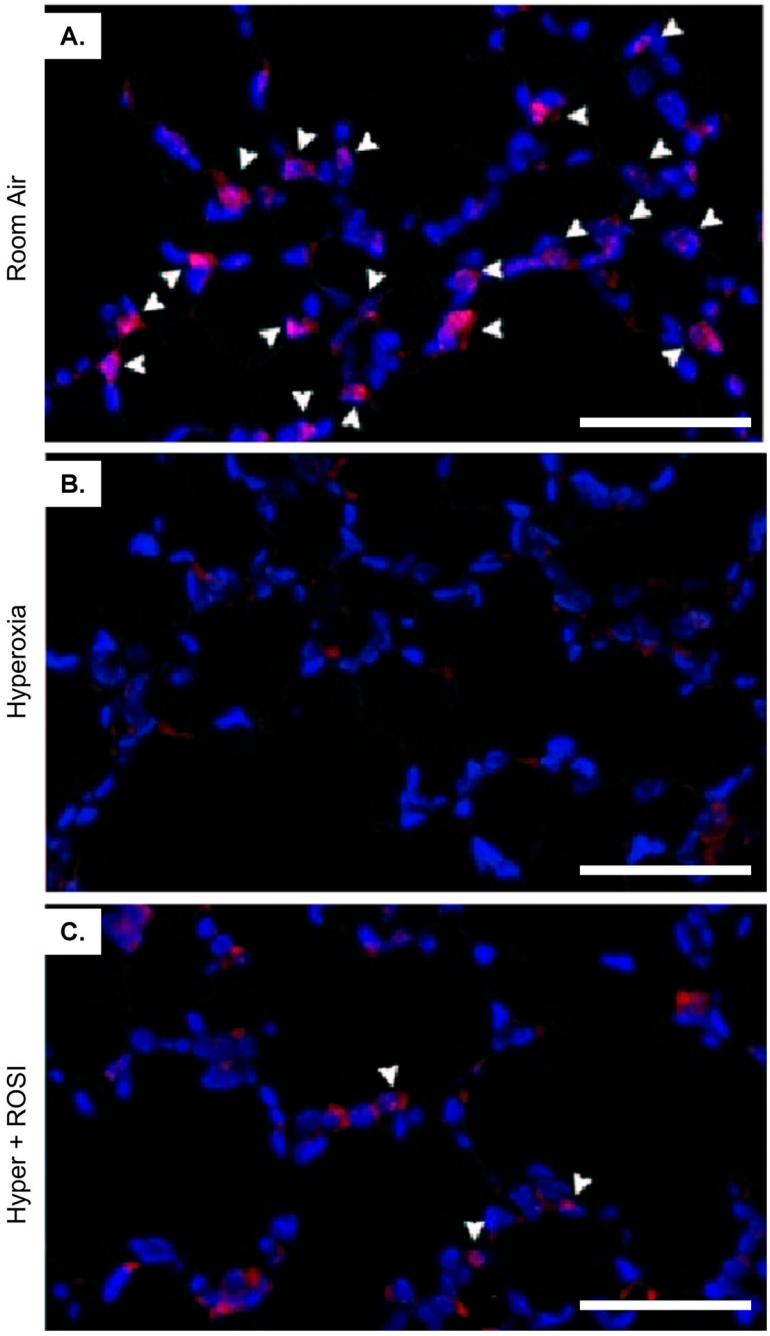

Figure 2. Nuclear Detection of PPAR-γ is Significantly Decreased in Lung Parenchymal Cells Following Neonatal Hyperoxic Exposure

Fluorescent immunostaining was performed to localize PPAR-γ expression on P13 at RA, in response to hyperoxic exposure and HE+ROSI. On P13 PPAR-γ protein expression was detected in nuclei of parenchymal cells adjacent to type II cells in the alveoli in the RA group (**A**). Expression was decreased in the hyperoxic exposed (**B**) and HE+ROSI (**C**) groups. PPAR-γ reactivity appeared pink indicated by arrow. Nuclei are DAPI stained and appear blue. Scale bar=50uM.

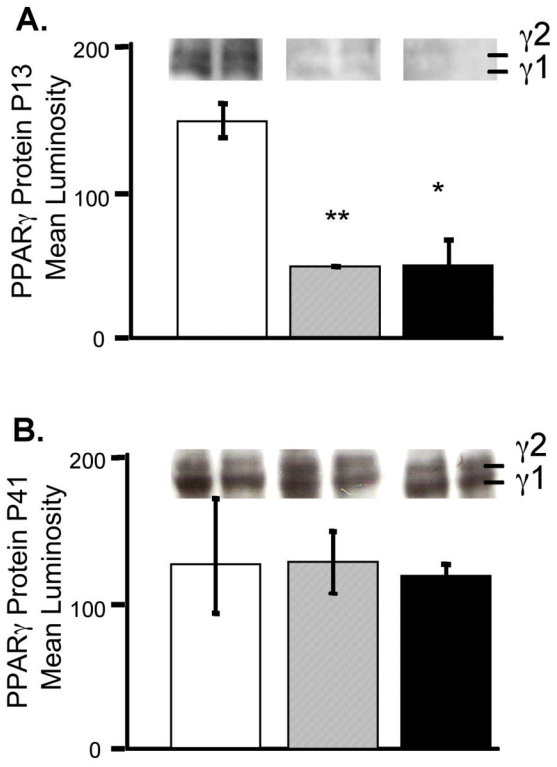

Figure 3. PPAR-γ Protein Expression Decreased in Lung Following Neonatal Hyperoxic Exposure

Histological differences in PPAR-γ expression on P13 (**A**) and P41 (**B**) were verified by Western blot analysis. Densitometry data was averaged from 6 mouse lungs per group collected in at least 2 separate experiments. The protein concentrations were standardized by protein assay and to β-actin. Average band intensities are presented. Error bars represent SEM. RA-white, HE-grey, HE+ROSI-black. *=Significantly different from the RA control unless indicated by bar. Lanes are representative of multiple blot results.

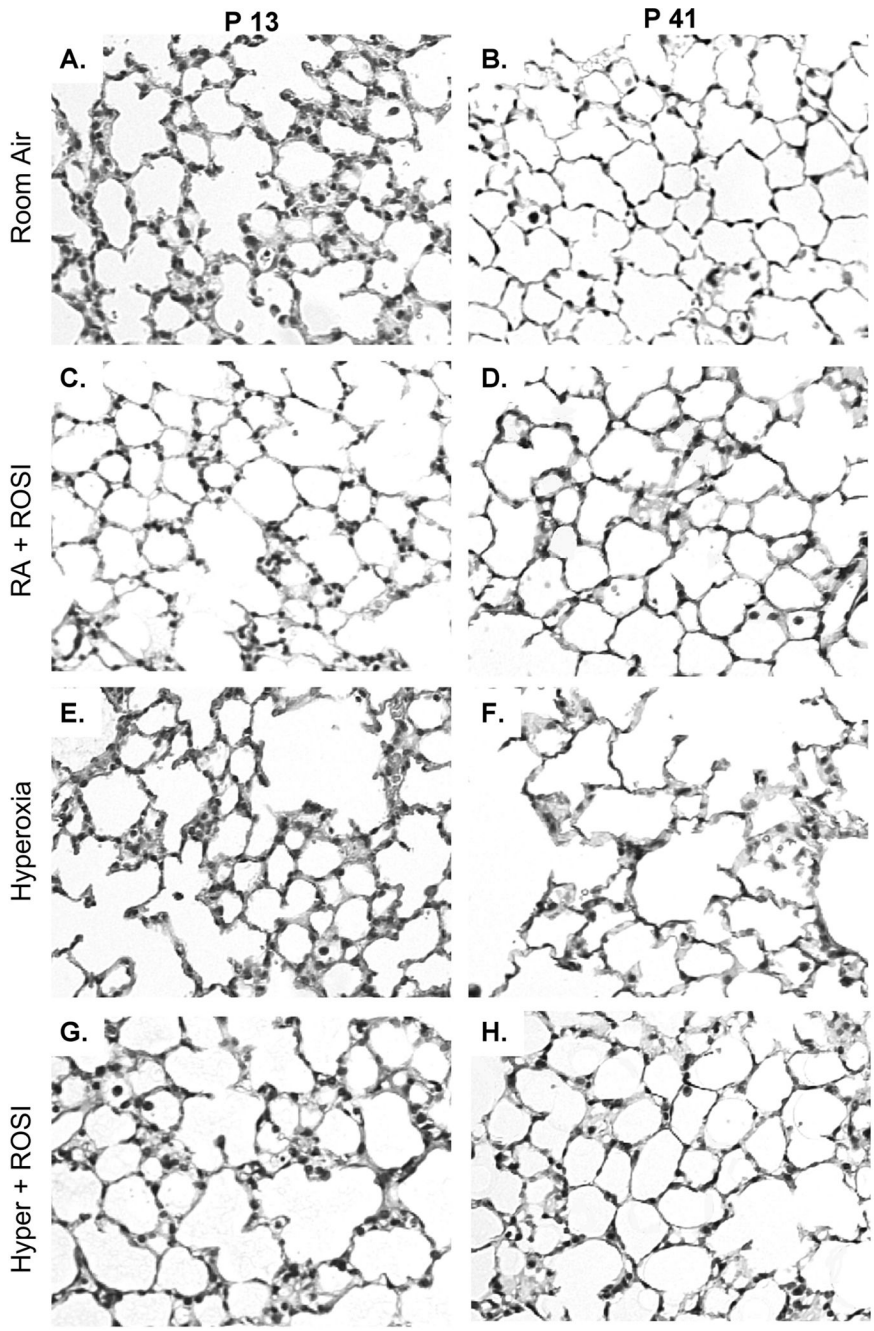

Figure 4. Systemic Administration of Rosiglitazone to Neonatal Mice Attenuates the Adverse Histological Effects of Hyperoxic Exposure in Developing Murine Lungs

Newborn mouse litters (postnatal day 0/1 of age) were exposed to RA or 70% oxygen for 10 days, a period corresponding to the late terminal saccular / early alveolar stages of lung development. The dams were fed a standard diet of chow impregnated with ROSI from P0 and litters exposed to RA or HE. Following HE animals were placed at RA. Moderate exposure of neonatal mice to hyperoxia during week one of life resulted in subtle changes in lung histology evident by hematoxylin and eosin stained lung tissue sections on P13 (**A vs E**) with lung simplification evident by P41 (**BvsF**). In contrast to HE alone ROSI+HE had

increased alveolar structures (**G&H**) and ROSI treatment during RA had no apparent effect on lung structure (**C&D**). Scale bar=50uM.

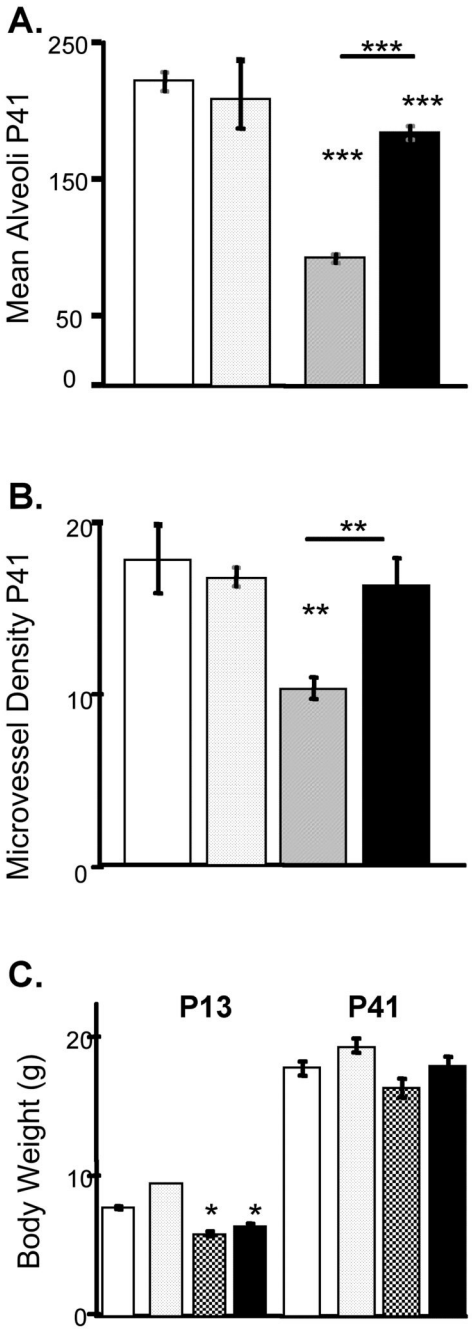

Figure 5. Quantitative Analysis of the Protective Effects of Rosiglitazone Against Hyperoxia in Developing Murine Lungs

Morphometric data was obtained over 5 independent experiments in which neonatal mice were exposed to moderate hyperoxia in the presence or absence of rosiglitazone as previously described. **A.** Alveolar density presented as mean +/- SEM number of alveoli per field of view. **B.** Microvessel density presented as mean +/- SEM. Mean Vessel counts per field of view determined by counting factor VIII positive microvessels. **C.** Mean body weights. RA-white, RA+ROSI-dotted, HE-grey, HE+ROSI-black. Error bars represent SEM. *=Significantly different from the RA control unless indicated by bar.

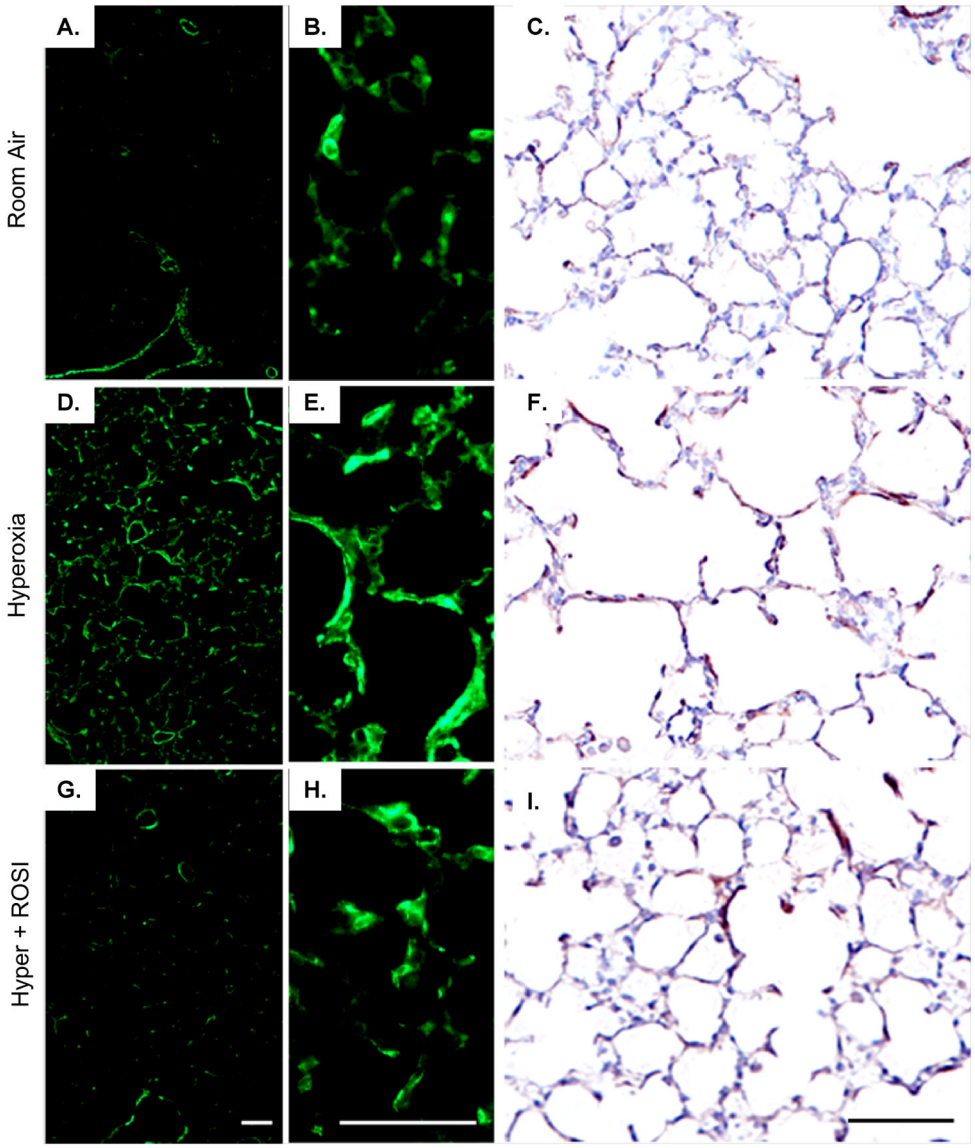

Figure 6. Myofibroblasts Increased with Hyperoxic Exposure in the Neonatal Lung on P13

α-SMA expression was localized by immunostaining following RA, HE and HE+ROSI. On P13 α-SMA protein expression was increased in the hyperoxic exposed and HE+ROSI groups relative to the RA group. Representative immunostained images of **A-C.** RA, **D-F.** HE, **G-I.** HE+ROSI. Positive α-SMA localization with immunofluorescent detection appeared green or DAB detection (CFI), brown. **B,E,H.** Respective enlargements of alveolar structures (from ADG). Scale bar=50uM.

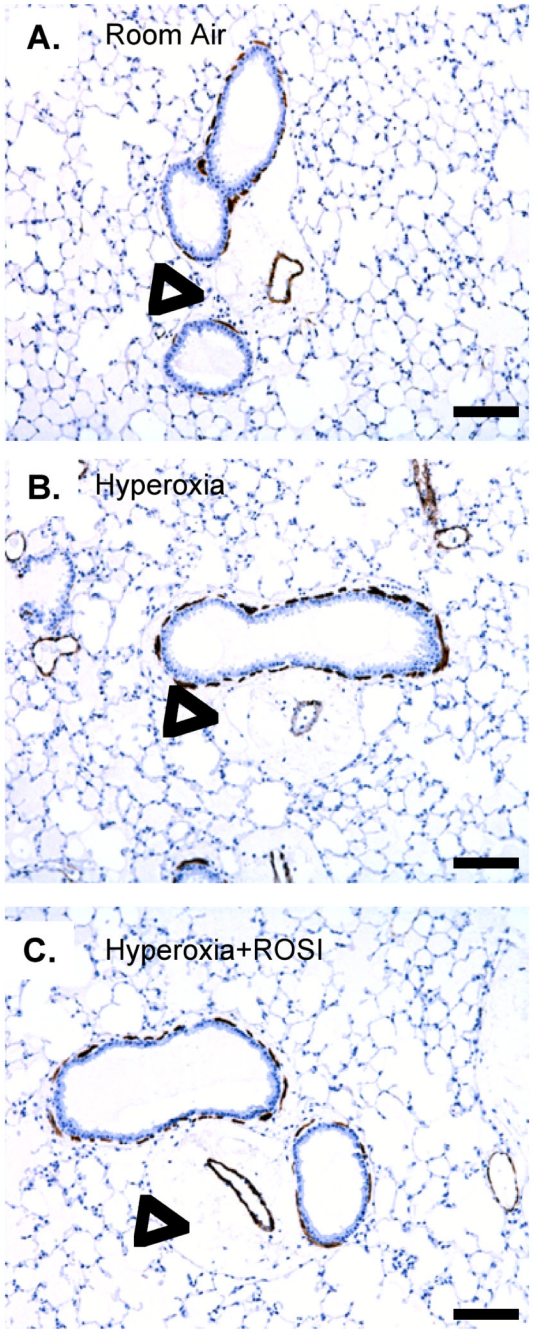

Figure 7. Adult Mice do not Exhibit Significant Smooth Muscle Remodeling or Chronic Inflammation following Neonatal Hyperoxic Exposure

α-SMA expression was localized by immunostaining on P41 following RA, HE and HE +ROSI. There was no evidence that HE resulted in significant airway smooth muscle remodeling or chronic inflammation relative to RA exposure. Representative images of **A.** RA, **B.** Hyperoxic exposed, **C.** HE+ROSI. Positive α-SMA localization appeared brown. Scale bar=50uM. Open arrow indicates where inflammatory cells would be localized as associated with airways and associated arteriole.

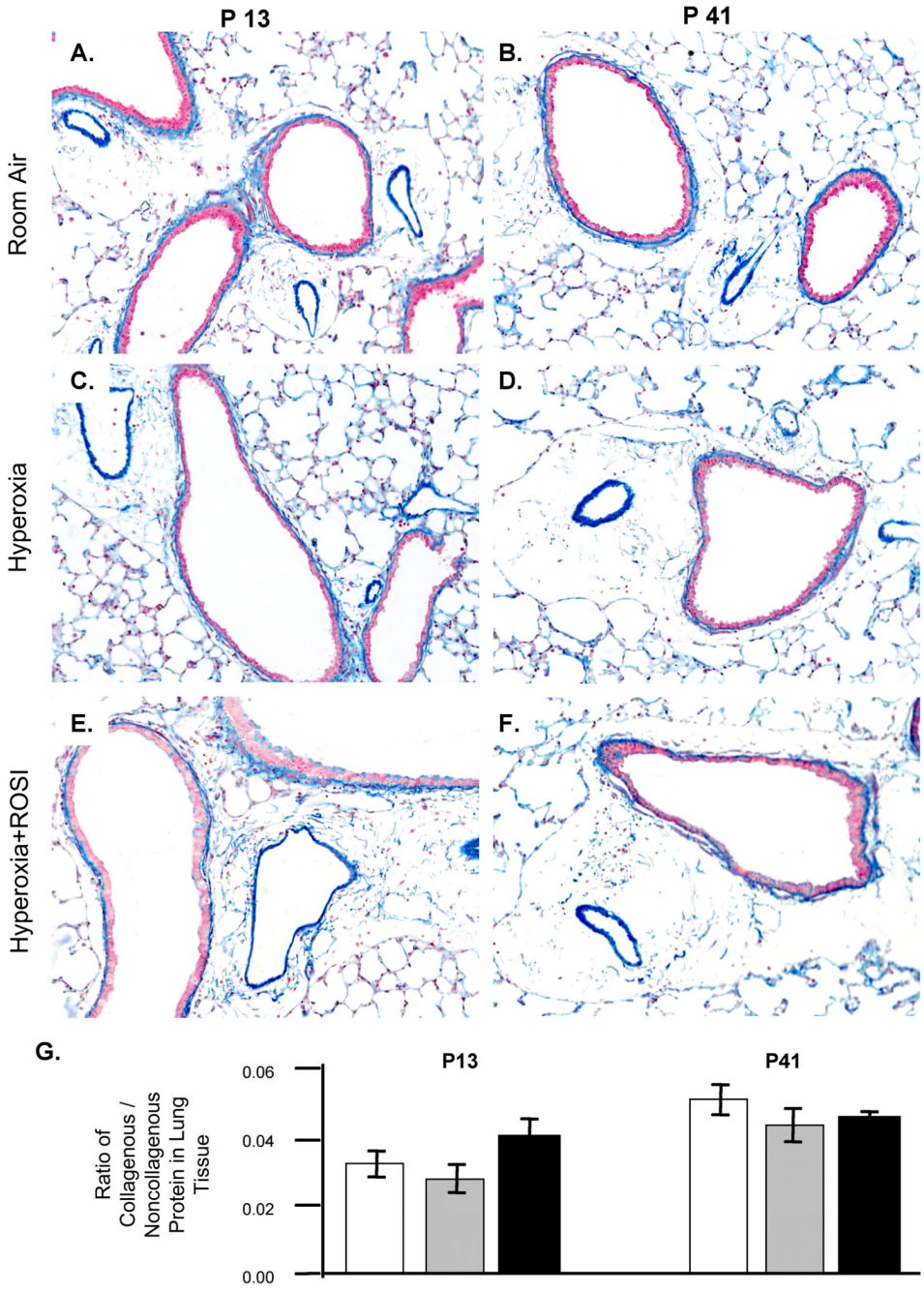

Figure 8. Collagen Accumulation was not Significantly Increased with Hyperoxic Exposure

The deposition of collagen was detected by Carstair's staining on P13 (A C E) and P41 (B D F). Collagen stained blue and was localized to interstitium, vessels and airways. The level of collagen accumulation following RA, HE and HE+ROSI was not significantly different (**G**). Scale bar = 50μM. RA-white, HE-grey, HE+ROSI-black.

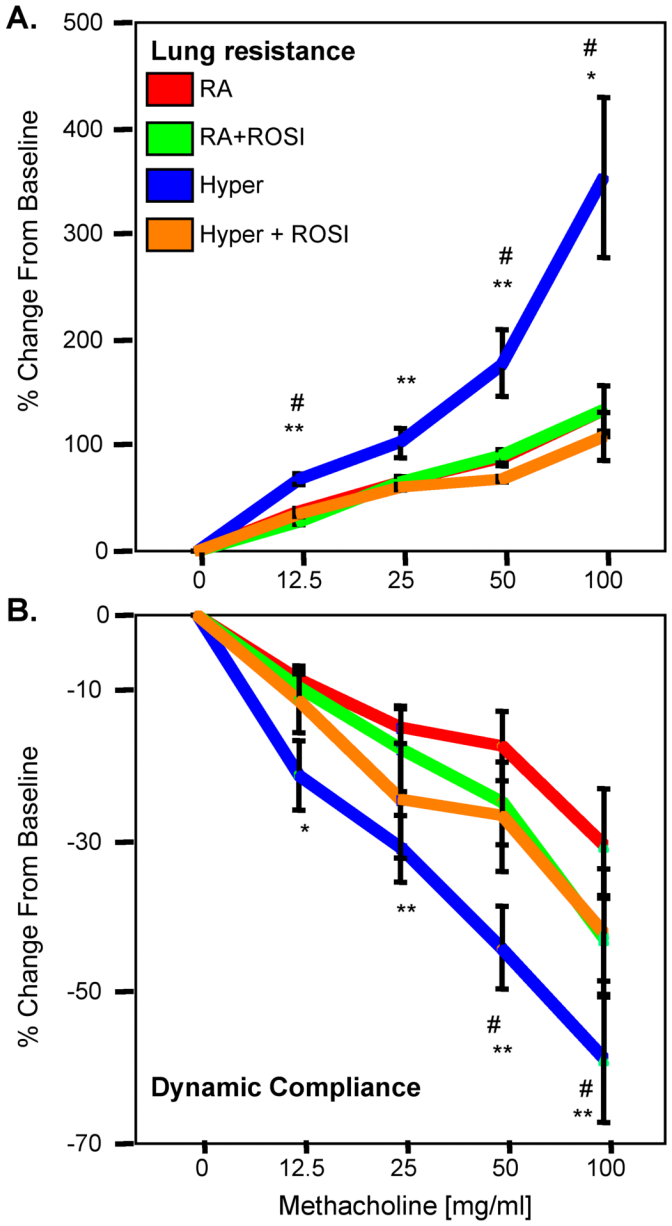

Figure 9. Neonatal Exposure to Hyperoxia Results in Adult Airway Hyperresponsiveness which was Attenuated with ROSI treatment

Measurements of airway resistance (**A**) and dynamic compliance (**B**) in response to methacholine (MCh) challenge were performed on mice having been exposed to RA, RA +ROSI, Hyperoxia or HE+ROSI on P55. Mice exposed to hyperoxia had significantly increased airway hypreresponsiveness (AHR) than the RA controls and HE+ROSI groups. In both cases the HE+ROSI group was not significantly different from the RA control groups.

Table 1

Name	P13 HE+ROSI Relative to RA	P13 HE+ROSI Relative to HE
ROSI Targets		
FBJ osteosarcoma oncogene	10.24	
frizzled homolog 4 (Drosophila)	2.14	
adiponectin receptor 2	1.74	
lipase, endothelial	3.74	1.64
lipin 1	3.41	1.92
Nuclear factor I/B	1.82	
phospholipase D1	1.5	
S100 calcium binding protein A8 (calgranulin A)		3.41
cyclin-dependent kinase inhibitor 1A (P21)		2.28

Table 2

Name	P13 HE	P13 HE+ROSI
CELL CYCLE		
Jun-B oncogene	1.93	3.93
H2A histone family, member X	-1.32	-1.61
cell division cycle 37 homolog (S. cerevisiae)	-1.79	-1.7
neuroblastoma myc-related oncogene 1	-1.59	-1.92
cyclin A2	-1.75	-3.13
cyclin B1	-2.39	-3.16
cyclin B2	-1.64	-2.41
cyclin D2	NC	-1.62
cyclin E2	-1.85	-3.56
cyclin T1	2.31	2.06
cyclin T2	1.72	1.46
cyclin-dependent kinase 4	-1.46	-1.58
cyclin-dependent kinase 6	1.29	NC
cyclin-dependent kinase inhibitor 2D (p19, inhibits CDK4)	-5.39	-9.1
cyclin-dependent kinase inhibitor 1A (P21)	NC	3.35
growth arrest and DNA-damage-inducible 45 gamma	2.26	2.38
BLOOD VESSEL DEVELOPMENT / ANGIOGENESIS & BRANCHING MORPHOGENESIS		
cysteine rich protein 61	2.17	3.14
connective tissue growth factor	1.32	1.5
serine (or cysteine) proteinase inhibitor, clade E, member 1	1.79	2.79
vascular endothelial growth factor C	1.39	1.63
fibroblast growth factor 1	1.32	1.46
roundabout homolog 4 (Drosophila)	1.49	1.46
neuropilin 1	1.45	1.5
ras homolog gene family, member B	1.38	NC
sema domain, seven thrombospondin repeats (type 1 and type 1-like), transmembrane domain (TM) and short cytoplasmic domain, (semaphorin) 5A	1.46	1.5
angiogenin, ribonuclease A family, member 1	1.4	1.53
type 1 tumor necrosis factor receptor shedding aminopeptidase regulator	1.55	1.49
ELK3, member of ETS oncogene family	2.06	NC
Angiopoietin 1	2.78	1.46
vascular endothelial growth factor C	1.39	1.63
thrombospondin 1	NC	1.36
endothelial differentiation sphingolipid G-protein-coupled receptor 1 (EDG1 or S1P1)	NC	1.95
endoglin	NC	1.61
connective tissue growth factor	1.32	1.5
endothelial differentiation sphingolipid G-protein-coupled receptor 1	NC	1.95

Name	P13 HE	P13 HE+ROSI
protein tyrosine phosphatase, receptor type, J	-2.47	-4.75
quaking	1.3	1.49
phosphatidic acid phosphatase type 2B	2.98	1.38
tumor necrosis factor, alpha-induced protein 2	NC	2.29
recombining binding protein suppressor of hairless (Drosophila)	NC	-1.46
ras homolog gene family, member B	1.38	1.66
c-fos induced growth factor	NC	1.51
endothelial PAS domain protein 1	NC	1.75
guanine nucleotide binding protein, alpha 13	1.46	1.61
transforming growth factor, beta 2	1.88	-1.34
FMS-like tyrosine kinase 1	1.63	2.32
WAS protein family, member 2	NC	1.5
angiogenin, ribonuclease A family, member 1	NC	1.71
Mitogen activated protein kinase 14	NC	-1.48
EXTRACELLULAR MATRIX		
CCAAT/enhancer binding protein (C/EBP), alpha	1.55	1.66
procollagen, type I, alpha 1	1.34	NC
procollagen, type XXVII, alpha 1	1.53	NC
procollagen, type I, alpha 2	2.11	NC
procollagen, type XXVII, alpha 1	1.79	NC

Table 3

Name	P13
BLOOD VESSEL MORPHOGENESIS	
cysteine rich protein 61	1.45
serine (or cysteine) proteinase inhibitor, clade E, member 1	1.56
thrombospondin 1	1.42
forkhead box F1a	1.69
endothelial differentiation sphingolipid G-protein-coupled receptor 1	1.77
inhibitor of DNA binding 1	1.47
guanine nucleotide binding protein, alpha 13	1.52
endoglin	1.34
cysteine rich protein 61	1.42
tumor necrosis factor, alpha-induced protein 2	2.16
recombining binding protein suppressor of hairless (Drosophila)	-1.32
thrombospondin 1	1.73
FMS-like tyrosine kinase 1	1.42
thrombospondin 1	1.74
forkhead box F1a	1.54
reticulon 4	-1.82
Quaking	-1.47
ELK3, member of ETS oncogene family	-3.15
Angiopoietin 1	-2.04
neuropilin 1	-5.2
MUSCLE DEVELOPMENT & CONTRACTION	
calponin 1	-1.71
tropomyosin 2, beta	-1.52
Titin	1.56
annexin A6	-1.82
myosin, heavy polypeptide 11, smooth muscle	-1.41
tropomyosin 1, alpha	-1.45
interferon-related developmental regulator 1 (IFRD1)	1.53
actin, alpha 2, smooth muscle, aorta	-1.39
myosin, light polypeptide 4	1.45
titin-cap	2.48
myosin, light polypeptide 3	1.75
mesenchyme homeobox 2 (Meox2)	-1.67
PATTERN SPECIFICATION & MORPHOGENESIS	
cysteine rich protein 61	1.45
B-cell translocation gene 2, anti-proliferative	1.92
ephrin B1	1.35

Name	P13
delta-like 1 (Drosophila)	1.46
homeo box A5	1.47
endothelin 1	1.47
CCAAT/enhancer binding protein (C/EBP), beta	1.35
ephrin B2	1.36
zinc finger and BTB domain containing 16	2.16
platelet derived growth factor receptor, alpha polypeptide	1.83
forkhead box F1a	1.69
peter pan homolog (Drosophila)	-1.56
WNT1 inducible signaling pathway protein 1	-1.44
forkhead box F1a	1.54
suppressor of cytokine signaling 3 (SOCS3)	1.66
Bone morphogenetic protein 1	2.09
Transforming growth factor, beta 2	-4.25
Angiopoietin 1	-2.04
RAR-related orphan receptor alpha	1.5
RESPONSE TO STIMULI	
CD14 antigen	1.6
early growth response 1 (Egr-1)	1.55
proliferating cell nuclear antigen	-1.34
chemokine (C-C motif) ligand 5 (CXCl5)	-1.56
chemokine (C-X-C motif) ligand 14 (CXCl14)	1.72
neutrophilic granule protein	4.14
chemokine (C-C motif) receptor 2 (CXCR2 or IL8R2)	-1.62
heat shock protein 1	1.54
caspase 3, apoptosis related cysteine protease	-1.35
chemokine (C-X-C motif) ligand 2 (CXCl2 or MIP2α)	6.3
Fas (TNF receptor superfamily member 6)	1.57

Table 3

Baseline Values for Pulmonary Function

Group	R_L	Cst	Damping	Elastance
	cm H_2O .ml^{-1}sec (SEM)	ml .cm H_2O^{-1} (SEM)	cm H_2O. ml^{-1} (SEM)	cm H_2O. ml^{-1} (SEM)
RA	0.27(.01)	0.081(.007)	6.37(.74)	31.6(2.9)
RA + ROSI	0.30(.03)	0.079(.005)	6.17(.52)	29.9(2.1)
Hyperoxia	0.30(.02)	0.076(.006)	5.50(.57)	30.0(2.3)
Hyper + ROSI	0.29(.02)	0.055(.008)	7.29(.74)	36.8(2.9)
	p<0.80	p<0.06	p<0.27	p<0.17